CT-based attenuation correction on the FLEX Triumph™ preclinical PET/CT scanner

Rameshwar Prasad, Mohammad R. Ay, *Member, IEEE*, Osman Ratib, and Habib Zaidi, *Senior Member, IEEE*

***Abstract*– Positron Emission Tomography (PET) has emerged as a very valuable molecular imaging modality for quantitative measurement of biochemical processes in the clinical and preclinical imaging domains. However, PET imaging suffers from various physical degrading factors including photon attenuation, which can be corrected using CT-based attenuation correction (CTAC) on combined PET/CT scanners. The attenuation map is calculated by converting CT numbers derived from low-energy polyenergetic x-ray spectra to linear attenuation coefficients at 511 keV. In this study, we implemented and evaluated tube voltage-dependent attenuation correction on the FLEX Triumph™ preclinical PET/CT scanner. The impact of both bilinear and quadratic polynomial calibration curve methods obtained at different CT tube voltages was assessed. Correlation coefficients and best fit equations were calculated for both techniques. Phantoms and rodents' PET images were used to assess improvements in image quality and quantitative accuracy. It was observed that the slopes of the bilinear calibration curves for CT numbers greater than 0 HU increase with increasing tube voltage. Significantly higher correlation coefficients were obtained using the quadratic polynomial calibration curve method. Acquired phantoms and rodents' PET data were successfully corrected for photon attenuation using the CTAC procedure thus enabling more accurate quantitative analysis of biochemical processes *in vivo*.**

I. INTRODUCTION

Positron Emission Tomography (PET) has emerged as a revolutionary molecular imaging technology for qualitative assessment and quantitative measurements of biochemical processes in the clinical and preclinical imaging domains. However, quantitative PET imaging suffers from many physical degrading factors with photon attenuation being one of the major issues impacting image quality and quantitative analysis of PET images. The magnitude of photon attenuation in small-animal PET is not as large as in clinical imaging. Indeed, 5 cm of soft tissue, the approximate transverse size of a 250 g rat, may absorb 40% of 511 keV photons. This proves that attenuation correction (AC) is still potentially important for quantitatively accurate estimation of tracer concentration in high-resolution small preclinical PET imaging [1]. Through knowledge of the attenuation properties of the object, the measurement along each line of response can be corrected for the photon attenuation [2]. Various strategies were developed for the purpose of attenuation correction purposes in PET [3]. CT-based attenuation correction (CTAC) is one well established techniques on combined PET/CT scanners owing to the low statistical noise and high-quality anatomical information, small crosstalk between PET annihilation photons and low energy x-rays, and higher throughput imaging protocols [4]. However, precise and accurate conversion of CT numbers derived from low-energy polyenergetic x-ray spectra from a CT scanner to linear attenuation coefficients at 511 keV has become essential in order to apply accurate CTAC to the acquired PET data. Several conversion strategies have been reported in the literature such as scaling [5], segmentation [6], hybrid (segmentation/scaling) [7] and piece-wise scaling [8].

The bilinear conversion method uses a linear relationship between CT numbers and linear attenuation coefficients of materials at 511 keV with one slope for soft regions (air-water segment) and another slope for bone regions (water–bone segment) [3, 4]. CT numbers in the range $-1000<H<0$ are considered to represent regions with a mixture of air and soft tissue and CT numbers $H> 0$ represent regions with mixture of soft tissue and bone. Other variants to the linear relationship were also proposed through the use of nonlinear regression like quadratic polynomial mapping algorithms [9].

Although the bilinear scaling conversion method remains the most widely used technique, the quadratic polynomial calibration curve method is an appealing approach. Calibration curve methods are generally calculated at a preset tube voltage and current. These methods are widely used and validated on clinical systems; however, they still need to be thoroughly investigated in high resolution small-animal PET imaging.

In this study, we implemented and evaluated tube voltage-dependent attenuation correction on the FLEX Triumph™ preclinical PET/CT scanner. We also assess improvements in image quality and quantitative capability of preclinical PET imaging corrected for attenuation using the tube voltage-dependent CTAC procedure where the attenuation map is generated using both bilinear and quadratic polynomial calibration curve methods.

II. MATERIALS AND METHODS

A. Data acquisition and processing

The data were acquired for all studies using commercially available the FLEX Triumph™ preclinical PET/CT scanner (Gamma Medica-Ideas, Nortridge, CA). The PET subsystem of this scanner uses BGO-based detector blocks having a 10

This work was supported by the Swiss National Foundation under grant No. 31003A-125246.

Rameshwar Prasad is with Division of Nuclear Medicine, Geneva University Hospital, CH-1211 Geneva, Switzerland (e-mail: rjhaji@gmail.com)

Mohammad Reza Ay is with the Department of Medical Physics and Biomedical Engineering, Tehran University of Medical Sciences, Tehran, Iran and Research Center for Science and Technology in Medicine, Tehran, Iran, and Research Institute for Nuclear Medicine, Tehran University of Medical Sciences, Tehran, Iran (e-mail: mohammadreza_ay@tums.ac.ir)

Osman Ratib is with the Division of Nuclear Medicine, Geneva University Hospital, CH-1211 Geneva, Switzerland (e-mail: osman.ratib@hcuge.ch)

Habib Zaidi is with the Division of Nuclear Medicine, Geneva University Hospital, CH-1211 Geneva, Switzerland (e-mail: habib.zaidi@hcuge.ch).

cm transaxial field-of-view (FOV), an 11.6 cm axial FOV, a central point source spatial resolution of 1.8 mm full-width at half-maximum (FWHM) and sensitivity near 8% at the center of the FIB. The CT subsystem includes a standard self-contained, air-cooled x-ray tube operating in the range of 40-80 kVp. PET scans were acquired with a 250–750 keV energy window and 12 ns timing window. Projection data are acquired in listmode format were first Fourier rebinned into 2D sinograms, and then reconstructed using 2D OS-EM algorithm (4 iterations and 10 subsets), resulting in 0.4×0.4×0.4 mm^3 voxel size for a 256×256×256 image volume. Fluorine-18 was used as radioisotope for PET studies. CT scans were acquired using CT tube voltages varying between 40 and 80 kVp and optimized tube current. The gantry rotated in continuous flying mode. A total of 512 projections were acquired in a full 360° scan with 2×2 binning and 1184×1120 projection matrix size. Images were reconstructed using modified 3D cone-beam Feldkamp algorithm resulting in 0.17×0.17×0.17 mm^3 voxel size for a 512×512×512 image volume. CT images were downsampled to match the matrix size of PET images. This was followed by energy conversion of CT images using experimentally obtained bilinear and quadratic polynomial calibration curve methods to match PET's energy. Gaussian smoothing was then applied using an appropriate kernel (FWHM = 1.8 mm) to match PET's spatial resolution. The created attenuation maps were then forward projected and exponentiated to generate attenuation correction factors (ACFs). The measured PET sinogram was then multiplied by the generated ACFs to obtain the attenuation corrected PET sinogram. The attenuation corrected PET sinogram was then reconstructed using 2D OS-EM algorithm (4 iterations and 10 subsets) to obtain the final CT-based attenuation corrected PET images. The CT-based AC procedure for preclinical PET imaging as shown in Fig. 1 was implemented in C++ programming language.

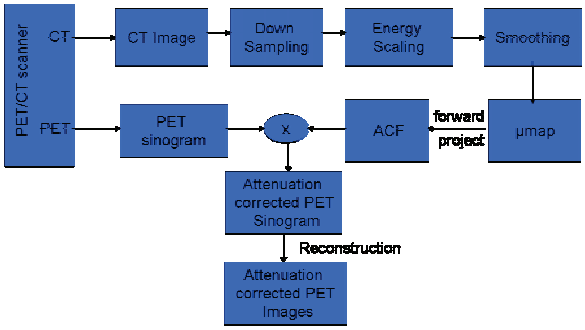

Fig. 1. Strategy for the implementation of CT-based attenuation correction.

B. Conversion of CT images to μmaps

A specially designed polyethylene cylindrical phantom (φ=70±0.5mm), containing 16 cylindrical holes (φ=5±0.1mm), was scanned on the CT sub-system of the preclinical PET/CT scanner by varying CT tube voltages between 40 to 80 kVp. To simulate different types of materials, thirteen syringes were filled with a mixed solution of K_2HPO_4 and water, with concentrations varying between 50 and 900 g/cm^3 along with three additional syringes containing water, air and lung equivalent tissue (Fig. 2). The CT image values were extracted from regions of interest (ROIs) in each image corresponding to the location of the calibration samples. The CT image values were then converted to CT numbers using the following equation:

$$CT_{number} = 1000 \times \left(\frac{I}{I_{water}} - 1 \right) \quad (1)$$

where I is the image intensity of a given voxel, and I_{water} is the CT number corresponding to water.

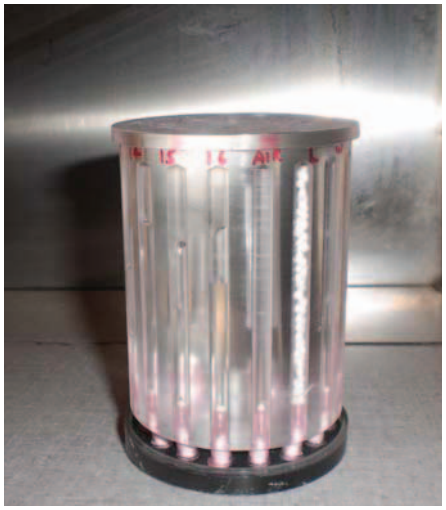

Fig. 2. Photograph of the in-house designed polyethylene cylindrical phantom containing 16 cylindrical holes.

Linear attenuation coefficients (LACs) for each material were calculated using the NIST data tables [10]. At CT energy level, Compton scattering dominates the LAC of low-Z materials (such as water and soft tissues), while photoelectric effect dominates LAC of high-Z materials (such as bone). Thus, different scaling coefficients were used to transform CT numbers into LACs (μ) at 511keV for different tissues:

The bilinear method is defined by the following equations:

$$\begin{aligned} \mu[cm^{-1}] &= 9.6\times10^{-5} \times (HU + 1000) \quad \forall\, HU \le 0 \\ \mu[cm^{-1}] &= a \times (HU + 1000) + b \quad \forall\, HU > 0 \end{aligned} \quad (2)$$

The quadratic method is defined by the following equations:

$$\begin{aligned} \mu[cm^{-1}] &= 9.6\times10^{-5} \times (HU + 1000) \quad \forall\, HU \le 0 \\ \mu[cm^{-1}] &= a \times (HU + 1000)^2 + b\times(HU + 1000) + c \quad \forall\, HU > 0 \end{aligned} \quad (3)$$

The bilinear and quadratic polynomial calibration curves were generated through regression analysis for fitting curves between LAC and CT numbers.

C. Validation studies

Two phantom studies were performed for validation purposes. A uniform cylinder phantom of 2.5 cm diameter and 14 cm length was filled with uniformly distributed mixture of water and 3 MBq of ^{18}F. The second is the NEMA NU 4-

2008 image quality phantom filled with 4 MBq of ^{18}F. The activity was measured with a dose calibrator. Rodents' studies included one mouse and one rat injected with ^{18}F-FDG. All PET studies, phantoms and rodents, were performed in an activity/count rate regime where random coincidences were almost negligible. Attenuation corrected PET images were compared to non-attenuation corrected PET images by drawing line profiles and though regions of interest based analysis. The recovery values *RV* for each AC method were calculated using the following equation:

$$RV = \left(\frac{ROI_{AC} - ROI_{NC}}{ROI_{NC}} \right) \quad (4)$$

where ROI_{AC}, ROI_{NC} are the mean values in a ROI drawn on the CT-based attenuation corrected image and on the uncorrected image, respectively. The percentage difference between images uncorrected and corrected PET images was also accessed for different PET studies.

III. Results

A. Conversion of CT images to μmaps

The CT Hounsfield units value for the different materials in the calibration phantom is plotted as a function of photon attenuation coefficient, and a least-squares fit was performed to determine the slopes as shown in Fig. 3.

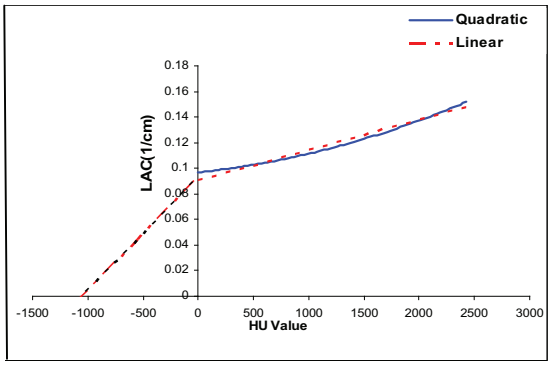

Fig. 3. Representative plots of the linear and quadratic fitting of the calibration curve at 70 kVp and 275 μA.

The fitting parameters and correlation coefficients (R^2) for both bilinear and quadratic calibration methods at different CT tube voltages are shown in Table 1. The transverse views of the attenuation maps of the NEMA image quality phantom and mouse, using both linear and quadratic calibration methods phantom are displayed in Fig. 4. Line profiles are also shown. Minor beam-hardening artifacts were visible in the quadratic-generated map.

B. Validation studies

Images of a transverse slice of the cylindrical phantom, NEMA NU 4- 2008 image quality phantom, rat and mouse studies are shown without and with attenuation correction in Figs. (5-8). Line profiles passing through a point near the center of the images are also shown. The recovery of the expected activity distribution achieved by the attenuation correction procedure is apparent.

The mean and coefficient of variation in the ROIs of uncorrected and corrected PET using bilinear and quadratic methods are shown in Table 2. The recovery values between CT corrected and uncorrected PET images are shown in Table 3.

Table 2. Comparison of mean and CV of PET studies for uncorrected and corrected (bilinear & quadratic methods) PET images.

Study	Uncorrected		Correction using bilinear method		Correction using quadratic method	
	Mean	CV (%)	Mean	CV (%)	Mean	CV (%)
Uniform Phantom	0.263	10.57	0.336	10.09	0.341	10.11
NEMA Phantom	1.364	5.21	1.877	5.17	1.880	5.17
Mouse	0.995	15.11	1.155	14.23	1.162	14.35
Rat	0.212	23.60	0.256	22.41	0.256	22.42

Table 3. Recovery values of attenuated corrected PET studies using bilinear and quadratic calibration methods.

Study	Recovery values	
	bilinear method	quadratic method
Uniform Phantom	0.178	0.189
NEMA Phantom	0.273	0.275
Mouse	0.159	0.164
Rat	0.359	0.367

IV. Discussion

Accurate quantification in PET requires a precise correction for the many physical degrading factors out of which attenuation correction is the major one. As the scanner installed in our facility was not equipped with CT-based attenuation correction, it was necessary to implement it on site. Our results show that CTAC resulted in reliable attenuation correction of PET images in the data sets of phantoms and rodents along used for validation purposes. In general, the improvement in recovery values is close to 17% for the uniform cylindrical phantom, 15 % for mouse and 35% for rat studies as shown in Table 3. These results are in agreement with results published in the literature [1,2].

Table 1. Summary of fitting parameters and correlation coefficients (R^2) for both bilinear and quadratic calibration methods.

kVp	Linear calibration method			Quadratic calibration method		
	$a(cm^{-1})(\times 10^{-5})$	$b(cm^{-1})(\times 10^{-2})$	R^2	$a(cm^{-1})(\times 10^{-9})$	$b(cm^{-1})(\times 10^{-6})$	R^2
40	1	8.6	0.897	3	0.7	9.58
50	2	8.6	0.901	4	0.3	9.62
60	2	8.62	0.886	5	3	9.73
70	9	9.2	0.98	6	9	9.69
80	9	8.8	0.926	6	6	9.31

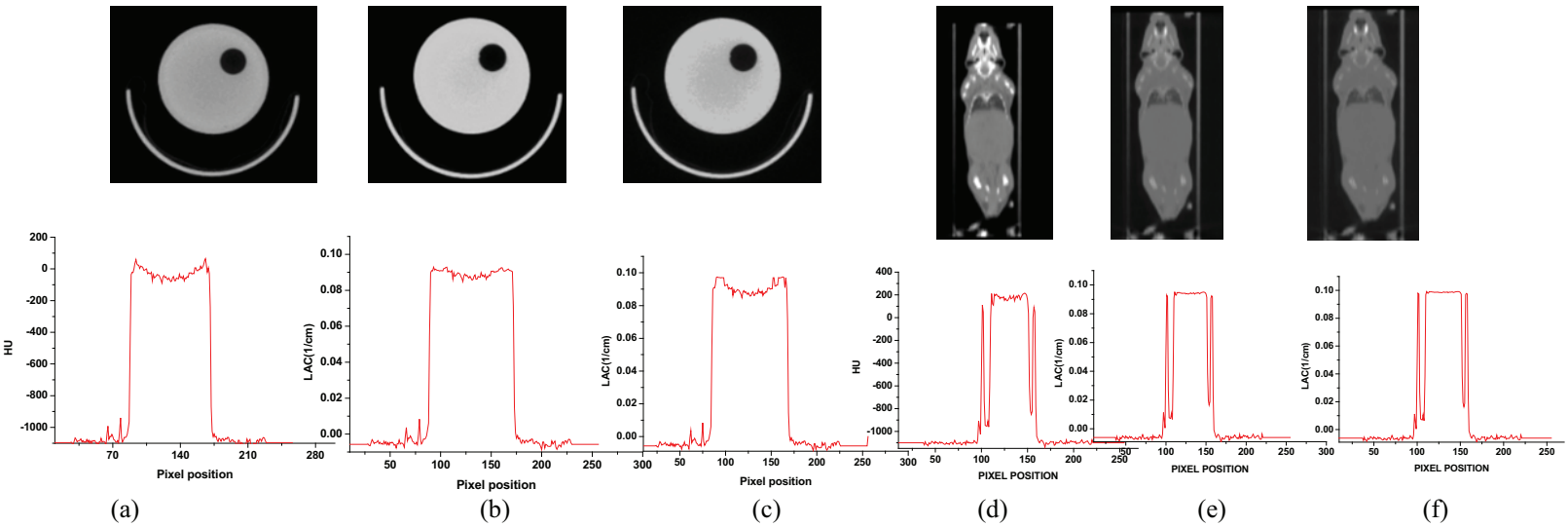

Figure 4. (a-c). Transaxial CT images of the NEMA phantom (upper row) showing the (a) original CT image (b) attenuation map using bilinear method(c) attenuation map using quadratic method and (lower row) corresponding line profiles. (d-f) Coronal CT images of the mouse (upper row) showing (a) the original CT image (b) attenuation map using bilinear method, (c) attenuation map using quadratic method and (lower row) their corresponding line profiles.

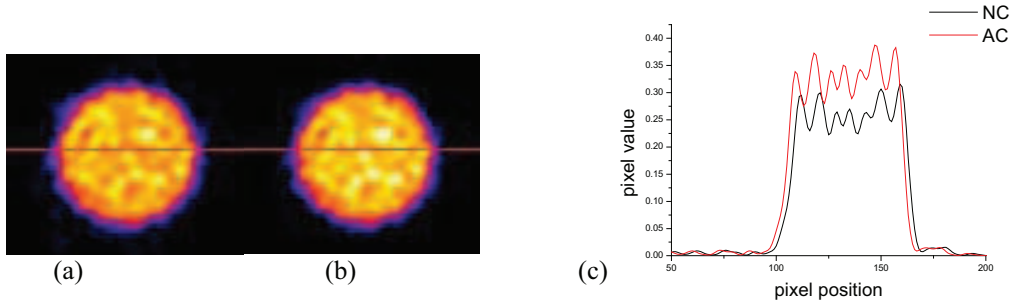

Figure 5. Transaxial PET image of the uniform cylindrical phantom showing: (a) Uncorrected (b) CT-based attenuated corrected, and (c) corresponding horizontal profiles through images shown in (a) and (b).

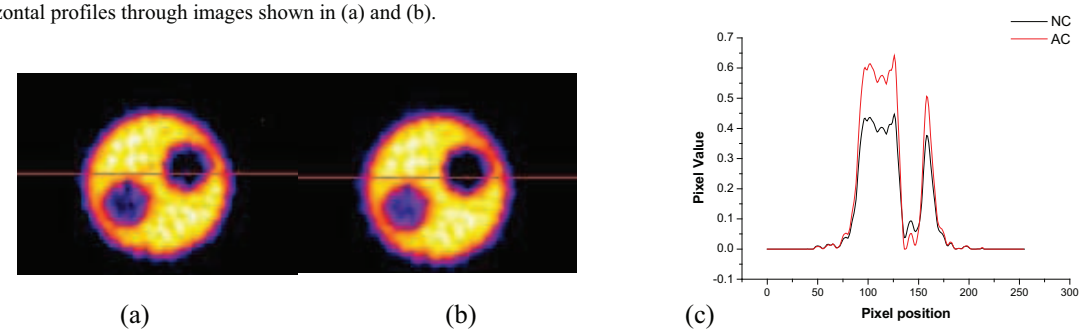

Figure 6. Transaxial PET image of the NEMA 2008 image quality phantom showing (a) Uncorrected, (b) CT-based attenuated corrected, and (c) Corresponding horizontal profiles through images shown in (a) and (b).

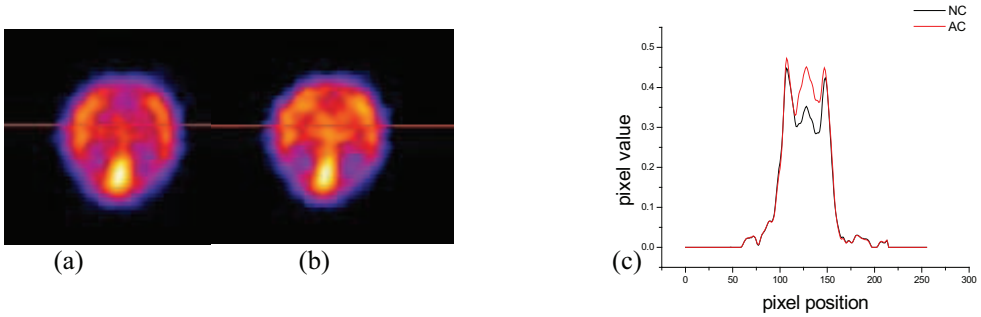

Figure 7. Transaxial PET image of a mouse showing (a) Uncorrected, (b) CT-based attenuated corrected, and (c) corresponding horizontal profiles through images shown in (a) and (b).

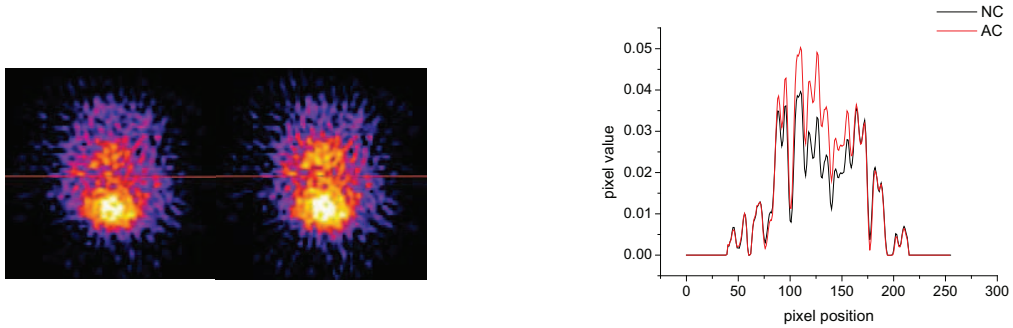

Figure 8. Transaxial PET image of a rat showing (a) Uncorrected, (b) CT-based attenuated corrected, and (c) corresponding horizontal profiles through images shown in (a) and (b).

The general applicability of CTAC has already been proven in small-animal PET imaging [1,2]. However, some pragmatic technical approached still need to be explored. The effect of varying CT tube voltages is investigated through quantitative analysis of created μ maps, generated ACFs and reconstructed PET data using experimental phantom and preclinical studies. Moreover, the practical application of calibration curve-based approaches for converting CT numbers to LAC is studied, using bilinear and quadratic calibration methods for water-bone segment. It was observed that increasing the tube voltage changes the slopes of calibration curves for HU greater than zero (Table 1). This can be explained as follows: the photoelectric interaction probability increases with decreasing tube voltage, particularly in materials with high atomic numbers. Moreover, calculation of calibration curves is based on the CT numbers of air, water and bone, the tube voltage dependence of bone's CT number can be the ground for the difference in the slopes of the calibration curves obtained at different CT tube voltages. Although there is some improvement in recovery values of different PET studies using the bilinear calibration and quadratic calibration methods, the difference between them does not appear to be significant. However, we considered only water-bone segment of calibration curves for deriving quadratic calibration curve analysis. The air-water segment of calibration curves was fitted linearly.

Despite the fact that the use of CTAC is certainly leading to more accurate quantification of high resolution preclinical imaging, further work is still needed to explore its broad potential.

V. Conclusion

It is concluded that significantly higher correlation coefficients were obtained using the quadratic polynomial calibration curve method comparison to the bilinear calibration method. It was also observed that the slopes of the calibration curves for CT numbers greater than 0 HU increase with increasing tube voltage. The use of quadratic calibration curve can provide better estimates of linear attenuation coefficients (LAC) than bilinear calibration method for PET quantitation. Attenuation correction is of prime importance in preclinical imaging. Acquired phantom and rodents' PET data were successfully corrected for photon attenuation using the CTAC procedure thus enabling more accurate quantitative analysis of biochemical processes *in vivo*.

Acknowledgements

This work was supported by the Swiss National Science Foundation under grant SNSF 3152A0-102143.

References

[1] R. Yao, J. Seidel, J.-S. Liow, and M. V. Green, "Attenuation correction for the NIH ATLAS small animal PET scanner.," *IEEE Trans Nucl Sci,* vol. 52, pp. 664-668, 2005.

[2] P. L. Chow, F. R. Rannou, and A. F. Chatziioannou, "Attenuation correction for small animal PET tomographs.," *Phys Med Biol,* vol. 50, pp. 1837-1850, Apr 21 2005.

[3] H. Zaidi, M-L. Montandon, A. Alavi, "Advances in attenuation correction techniques in PET," PET Clin. vol. 2, pp. 191-217, 2007.

[4] J. Yu, J. Seidel, M. Pomper, and B. M. W. Tsui, "Experimental evaluation of the bilinear transformation used in the CT-based attenuation correction for small animal PET imaging," in *Nuclear Science Symposium Conference Record, 2007. NSS '07. IEEE*, 2007, pp. 3747-3750.

[5] T. Beyer, P. E. Kinahan, D. W. Townsend, and D. Sashin, "The use of X-ray CT for attenuation correction of PET data," in *Proc. IEEE Nuclear Science Symposium and Medical Imaging Conference*, 30 Oct.-5 Nov., Norfolk, VA, USA, 1994, pp. 1573-1577.

[6] P. E. Kinahan, B. H. Hasegawa, and T. Beyer, "X-ray-based attenuation correction for positron emission tomography/computed tomography scanners.," *Semin Nucl Med,* vol. 33, pp. 166-179, Jul 2003.

[7] P. E. Kinahan, D. W. Townsend, T. Beyer, and D. Sashin, "Attenuation correction for a combined 3D PET/CT scanner.," *Med Phys,* vol. 25, pp. 2046-2053, Oct 1998.

[8] C. Bai, L. Shao, A. J. Da Silva, and Z. Zhao, "A generalized model for the conversion from CT numbers to linear attenuation coefficients.," *IEEE Trans Nucl Sci,* vol. 50, pp. 1510-1515, 2003.

[9] M. Shirmohammad, M. Ay, A. Rahmim, S. Sarkar, H. Zaidi, "Comparative assessment of different energy mapping approaches in CT based attenuation correction: a patient study," IFMBE Proceedings. J. Vander Sloten PV, M. Nyssen, J. Haueisen, Eds, Antwerp, Belgium, 23-27 November 2008: Springer; 2008; pp 496–499.

[10] M. J. Berger, J. H. Hubbell, S. M. Seltzer, J. Chang, J. S. Coursey, R. Sukumar, and D. S. Zucker, "XCOM: photon cross sections database. Report NBSIR 87-3597" Gaithersburg: Ionizing Radiation Division, Physics Laboratory, National Institute of Standards and Technology, Gaithersburg, MD 20899.